Nanoscale Advances

ROYAL SOCIETY OF CHEMISTRY

PAPER

View Article Online
View Journal | View Issue

Cite this: *Nanoscale Adv.*, 2023, **5**, 5399

Box–Behnken design of thermo-responsive nano-liposomes loaded with a platinum(IV) anticancer complex: evaluation of cytotoxicity and apoptotic pathways in triple negative breast cancer cells†

Nada K. Sedky,[a] Maria Braoudaki,[b] Noha Khalil Mahdy,[c] Kenzy Amin,[d] Iten M. Fawzy,[e] Eleni K. Efthimiadou,[f] Rana A. Youness[gh] and Sherif Ashraf Fahmy *[d]

Herein, thermo-responsive liposomes (TLs) loaded with Asp (Asp/TLs) were produced by self-assembling DPPC, DSPE-PEG2000, and cholesterol. The preparation variables were optimized using the Box–Behnken design (BBD). The optimized Asp/TLs exhibited an average particle size of 114.05 ± 1.56 nm, PDI of 0.15 ± 0.015, zeta potential of −15.24 ± 0.65 mV, and entrapment efficiency (EE%) of 84.08 ± 2.75%. In addition, under physiological conditions, Asp/TLs showed spherical shape, outstanding stability and thermo-triggered the release of Asp at 38 °C, reaching the maximum Asp release at 40 °C. The MTT assay showed that the optimal Asp/TLs exhibited the highest cytotoxic activity upon exposure to mild hyperthermia (40 °C) against the invasive triple-negative breast cancer cell line (MDA-MB-231) when compared to other preparations. The IC_{50} of Asp/TLs (40 °C) was estimated at 0.9 μg mL^{-1}, while that of free Asp (40 °C) was 3.83 μg mL^{-1}. As such, the optimal Asp/TLs were shown to increase the cytotoxic activity of Asp by 4-fold upon exposure to mild hyperthermia. The IC_{50} values of Asp and Asp/TLs without exposure to 40 °C were 6.6 μg mL^{-1} and 186 μg mL^{-1}, respectively. This indicated that Asp was released only when placed at 40 °C. The apoptosis assay revealed that Asp/TLs (40 °C) caused a remarkable increase in the percentage of cell population among both the late apoptosis and necrosis quartiles, as well as a significant decline in the viable cell quartile ($P \leq 0.001$) when compared to Asp (40 °C). Asp/TLs (40 °C) and Asp (40 °C) could stimulate the intrinsic apoptosis pathway by upregulating the apoptotic genes *Bak* and *Bax*, while downregulating the anti-apoptotic genes, *BCL-xL* and *BCL-2*. The free Asp (40 °C) increased the gene expression of *Bak* and *Bax* by 4.4- and 5.2-folds, while reducing the expression of *BCL-xL* and *BCL-2* by 50% and 73%, respectively. The optimal Asp TLs (40 °C) manifested more potent effects as demonstrated by the upregulation of *Bak*, *Bax*, and *P53* by 5.6-, 7.2-, and 1.3-folds, as well as the downregulation of *BCL-xL* and *BCL-2* by 70% and 85%, respectively. As such, the optimal Asp TLs (40 °C) treatment displayed the most potent cytotoxic profile and induced both apoptosis and necrosis in MDA-MB-231.

Received 28th May 2023
Accepted 29th August 2023

DOI: 10.1039/d3na00368j

rsc.li/nanoscale-advances

1. Introduction

For decades, tremendous pressure has been imposed on the pharmaceutical industry and research groups to improve the quality of cancer treatment, which remains on the top list of fatal diseases responsible for high mortality rates.[1] Previous reports showed that more than 18 million patients are diagnosed with cancer yearly, leading to worrisome cancer trends.[1,2]

[a]*Department of Biochemistry, School of Life and Medical Sciences, University of Hertfordshire Hosted by Global Academic Foundation, R5 New Garden City, New Administrative Capital, Cairo, Egypt*

[b]*Department of Clinical, Pharmaceutical, and Biological Science, School of Life and Medical Sciences, University of Hertfordshire, Hatfield AL10 9AB, UK*

[c]*Department of Pharmaceutics and Industrial Pharmacy, Faculty of Pharmacy, Cairo University, Kasr El-Aini Street, 11562 Cairo, Egypt*

[d]*Department of Chemistry, School of Life and Medical Sciences, University of Hertfordshire Hosted by Global Academic Foundation, R5 New Garden City, New Capital, Cairo 11835, Egypt. E-mail: sheriffahmy@aucegypt.edu; Tel: +20-1222613344*

[e]*Department of Pharmaceutical Chemistry, Faculty of Pharmacy, Future University in Egypt, 11835 Cairo, Egypt*

[f]*Inorganic Chemistry Laboratory, Department of Chemistry, National and Kapodistrian University of Athens, Panepistimiopolis, Zografou 157 71, Greece*

[g]*Biology and Biochemistry Department, Faculty of Biotechnology, German International University (GIU), New Administrative Capital, Cairo, Egypt*

[h]*Department of Biology and Biochemistry, School of Life and Medical Sciences, University of Hertfordshire Hosted by Global Academic Foundation, R5 New Garden City, New Administrative Capital, Cairo, Egypt*

† Electronic supplementary information (ESI) available. See DOI: https://doi.org/10.1039/d3na00368j

Several chemotherapeutic groups have been used in breast cancer therapy, for which more than 50% of breast cancer patients are treated with platinum-based antineoplastic drugs (PDs),[3,4] such as cisplatin (Fig. 1A), carboplatin (Fig. 1B) and oxaliplatin (Fig. 1C).[5,6] Cisplatin, the first generation PD that was sold under the brand name Platinolwas, was approved by the US Food and Drug Administration (FDA) for treating a broad spectrum of solid tumors in 1978.[7] Its mechanism of action depends on the formation of DNA adducts, leading to intra-strand and interstrand crosslinks and, subsequently, distorting the DNA of cancer cells and inducing apoptosis. Also, cisplatin promotes programmed apoptosis by inhibiting DNA replication and transcription.[8]

Aside from cisplatin's desirable cytotoxic features in treating various cancer types, its drawbacks lie in its non-selective therapeutic actions causing systemic toxicity.[4] In an attempt to improve the chemotherapeutic efficiency, minimize toxic effects, and overcome issues of multiple resistance, the FDA-approved second and third generations of PDs, such as carboplatin and oxaliplatin, respectively, were developed based on cisplatin,.[9,10] Also, prodrugs were designed by tethering chemical groups to the platinum center of cisplatin. For instance, asplatin (Asp), *c*,*c*,*t*-[$PtCl_2(NH_3)_2$(OH)(acetylsalicylic acid)] (Fig. 1D), is synthesized by conjugating acetylsalicylic acid to the cisplatin molecule *via* the Pt center.[11,12] Asp is a Pt(IV) complex that, unlike Pt(II) ones, is more inert and shows much lower adverse effects. When Asp is taken up by cells, it is transformed into the active form, Pt(II), by intracellular reductants such as glutathione.[12] The active Pt(II) induces apoptosis by activating the BCL-2 mitochondrial pathway, and upregulating *BAX* and *BAK* genes.[11–13] In addition, Asp demonstrated higher cytotoxicity than cisplatin against different cancer cells, and showed the ability to kill cisplatin-resistant cancerous cells.[13,14] Yet, Asp still has several limitations, such as chemoresistance preventing clinical translation. In addition, one further limitation is the premature conversion into the Pt(II) active species by the reductants in the bloodstream, before reaching tumor tissue, leading to reduced therapeutic action and systemic toxic effects.

Novel nanoformulation approaches have been introduced to increase the selectivity and efficacy of chemotherapeutics, and might revive interest in PDs with restricted approval, such as Asp. Liposomes are considered one of the promising nanocarriers for effectively delivering various chemotherapeutics. Liposomes are formed from a hydrophilic core surrounded by one or multiple bilayers of cholesterol and phospholipids.[15,16] Thus, liposomes can accommodate both hydrophilic and hydrophobic therapeutic agents inside their central compartment and/or the outer lipid bilayer. Liposomes are biocompatible and could enhance the bioavailability, solubility, and targeting capability of their payloads.[16–21] Several studies reported the encapsulation of various chemotherapeutics into liposomes, such as paclitaxel,[20] doxorubicin,[20,21] and nedaplatin.[22] Moreover, long-circulating thermo-responsive liposomes (TLs) were designed using a blend of heat-sensitive phospholipids such as 1,2-dipalmitoyl-*sn*-glycero-3-phosphocholine (DPPC), and polyethylene (PEG) grafting agents such as *N*-(carbonylmethoxypolyethylene glycol2000)-1,2-distearoyl-*sn*-glycero-3-phosphoethanolamine ($mPEG_{2000}$-DSPE).[22,23] The presence of $mPEG_{2000}$-DSPE makes liposomes stealthy by creating an outer layer of polymeric chains on the TLs exterior surface, which serves as a hydrophilic barrier that hinders the interaction of TLs with proteins (mainly opsonins). This protects TLs from being recognized by the reticular endothelial system (RES) and hence reduces their opsonization, extending their circulation time and boosting their stability. In addition, stealthy TLs could extravasate and passively accumulate inside tumor cells by the enhanced permeability and retention (EPR) effect.[22,23] Then, when the intratumor TLs are subjected to mild local hyperthermia (38–42 °C), they are disassembled through the phase transition conversion from a solid gel phase to a liquid one, and eventually release their payloads.[23,24] Furthermore, combining mild hyperthermia with chemotherapy as an adjunctive therapy has been reported to boost the anticancer effects on different types of cancers,[25–27] including breast,[28] skin,[29] and bladder[30] cancers.

In this study, asplatin-loaded thermo-responsive liposomes (Asp/TLs) were prepared by the thin film approach employing

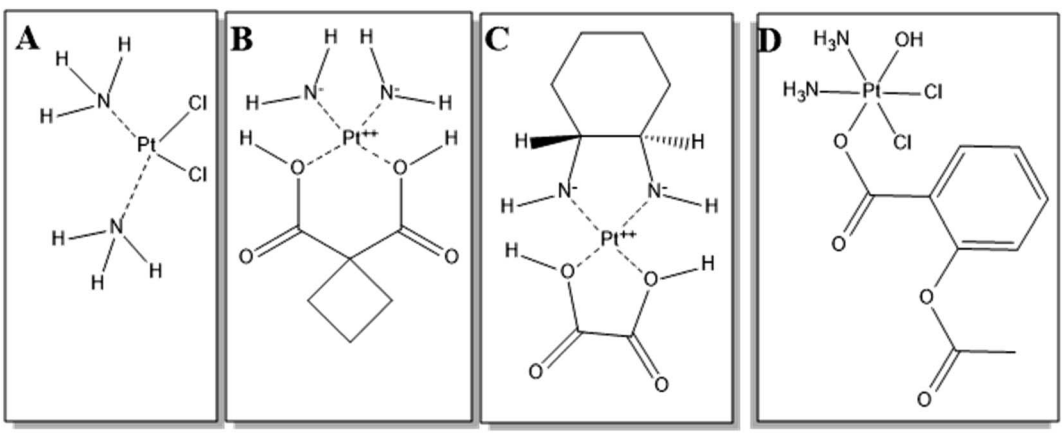

Fig. 1 Chemical structures of (A) cisplatin, (B) carboplatin, (C) oxaliplatin, and (D) asplatin. The structures were drawn using ChemDraw Pro 12.0.

a blend of phospholipids [1,2-dipalmitoyl-*sn*-glycero-3-phosphocholine (DPPC), and 1,2-distearoyl-*sn*-glycero-3-phosphoe-thanolamine-*N*-[maleimide(polyethylene glycol)-2000] (ammonium salt) (DSPE-PEG-2000)] as the main liposomal backbone phospholipids and cholesterol. The formulation variables were optimized using a 3^3 Box–Behnken surface response design (BBD). The tested factors were cholesterol; 2 DPPC, DSPE-PEG 2000 : 2 DPPC, and lipids : drug molar ratios. In this BBD, we focused on responses such as average particle size (PS), polydispersity index (PDI), zeta potential (ZP), and entrapment efficiency (EE). Then, the factors' main effects and interactions were analyzed to estimate the level of each factor to prepare the optimized formulation. The optimized formulation was further investigated in terms of shape, entrapment efficiency (EE%), stability, and temperature-dependent release manner. Asp/TLs were also evaluated for their biological activity on the invasive triple-negative breast cancer cell line, MDA-MB-231. Cellular viability, apoptosis, and molecular biology assays were performed to examine the effects of the optimal Asp/TLs on MDA-MB-231 cells, especially when exposed to mild hyperthermia (40 °C).

2. Materials and methods

2.1. Materials

1,2-Dipalmitoyl-*sn*-glycero-3-phosphocholine (DPPC), 1,2-distearoyl-*sn*-glycero-3-phosphoe-thanolamine-*N*-[maleimide(polyethylene glycol)-2000] (ammonium salt) (DSPE-PEG-2000), and cholesterol were purchased from Avanti Polar Lipids, Inc., USA. Dulbecco's modified Eagle's medium DMEM, the antibiotic-antimycotic, and L-glutamine were purchased from Lonza (Switzerland). Fetal bovine serum was obtained from Gibco (Germany). All other analytical-grade chemicals were obtained from Sigma-Aldrich (Germany).

2.2. Synthesis of asplatin

The synthesis and characterization of asplatin were carried out as described in our previously reported method.[12]

2.3. Experimental design

Three-factor, three-level (3^3) Box–Behnken experimental design (BBD, Design-Expert® software, Version 12, Stat-Ease Inc., Suite 480 Minneapolis, MN 55413) was utilized to optimize the development of Asp-loaded TLs statistically. The three independent variables included cholesterol : 2 DPPC molar ratio (denoted by A), DSPE-PEG 2000 : 2 DPPC molar ratio (denoted by B), and lipids : drug molar ratio (denoted by C). As demonstrated in Table 1, the levels of these variables were selected as (−1, 0, and +1), corresponding to low, middle, and high levels, respectively. The dependent variables (responses) involved were particle size (Y1), polydispersity index (Y2), zeta potential (Y3), and entrapment efficiency percentage (Y4). The ranges of the low and high levels for each independent factor were chosen by relying on initial trials that were carried out to determine the optimized Asp/TLs. Afterward, based on the selected low and high levels, the software automatically generated the medium levels of the three variables. The experimental design involved 17 trials (relying on the BBD output), with five center point repetitions. The composition of the 3^3 Box–Behnken experimental design for preparing Asp/TLs is shown in Table S1.† Analysis of variance (ANOVA) was utilized to evaluate the model statistically, and p-values <0.05 were considered significant.

2.4. Preparation of thermo-responsive liposomes loaded with asplatin (Asp/TLs)

Relying on the findings of the 3^3 BBD, 17 different Asp/TLs formulae were developed using the thin-film hydration approach[29,30] employing different molar ratios of DPPC, cholesterol, and DSPE-PEG2000, as presented in Table S2.† The lipid mixture and Asp were dissolved in a mixture of chloroform/methanol (2 : 1, v/v). The formed solution was then evaporated under a vacuum for 60 min using a rotary evaporator working at 53 °C, generating a thin lipid film. Then, the generated thin film was hydrated using phosphate buffer saline (pH 7.4) for 45 min at 53 °C, followed by bath sonication for 2 min, forming the multilamellar vesicles. In order to produce monodispersed unilamellar vesicles with reduced size and polydispersity index, the suspension was extruded through a polycarbonate membrane (100 nm pore size) for 12 cycles at 53 °C (AvantiMini-Extruder from Avanti Polar Lipids, Inc., USA). The free drug was removed using ultracentrifugation, and then the prepared TLs were kept at 4 °C until further investigations. The same protocol was used to prepare empty TLs without adding Asp.

2.5. Measurements of particle size, polydispersity index (PDI), and zeta potential

The particle sizes, PDI, and zeta potentials of all TL formulations were measured at 25 °C *via* dynamic light scattering technique by means of a Zetasizer Nano ZS (Malvern Instruments, Herrenberg, Germany).[31]

Table 1 Independent parameters and their related levels of the 3^3 BBD for Asp/TLs preparation, and their levels corresponding to the optimized Asp/TLs formulation

Independent parameters		Levels of factors			
		Low (−1)	Medium (0)	High (+1)	Optimized levels
A	Cholesterol : 2 DPPC molar ratio	0.5 : 2	1 : 2	1.5 : 2	0.5 : 2
B	DSPE-PEG 2000 : 2 DPPC molar ratio	0.13 : 2	0.26 : 2	0.39 : 2	0.39 : 2
C	Lipid : drug molar ratio	5 : 1	12.5 : 1	20 : 1	5 : 1

2.6. Calculation of entrapment efficiency (EE%)

The EE% of all Asp/TLs formulations was conducted using the direct method, as previously reported,[32] with few modifications. In brief, an aliquot of Asp/TLs was ultracentrifuged for 2 h at 12 000 rpm. Afterward, the residue was separated, dissolved in an HCl solution (1 mol L^{-1}), and subjected to vortex stirring. Then, Asp was quantified spectrophotometrically at 283 nm using a dual-beam spectrophotometer (Peak instruments T-9200, USA). Finally, the EE% of all Asp/TLs was calculated utilizing eqn (1) shown below.

$$\text{Entrapment efficiency } (\%) = \frac{\text{Entrapped amount of Asp}}{\text{Initial amount of Asp}} \times 100 \quad (1)$$

2.7. Formulation optimization

Design-Expert 12® software (Version 12, Stat-Ease Inc., Minneapolis, MN, USA) was utilized to verify the optimum Asp/TLs preparation through statistical optimization of the variables. The precise constraints applied to the particle size, PDI, zeta potential, and EE% are shown in (Table 3). The developed optimum formulation was prepared and characterized to verify the validity of the selected models for all the factors tested and their responses-predicting ability. In this context, one prediction point was conducted, and the software averaged the response data. As described in Section 2.4, the optimized formula was prepared in triplicate for further studies.

2.8. Investigating the optimal Asp/TLs

2.8.1. Morphological features and UV-vis analysis. The size and morphological features of the optimal Asp/TLs formulation were evaluated utilizing transmission electron microscopy (TEM, JEOL-JEM 2100) electron microscope (Musashino, Akishima, Tokyo, Japan). Then, a histogram was constructed illustrating the mean particle size (nm) of the optimal Asp/TLs, employing the image processing program Image J (NIH, Bethesda, MD, USA). The successful incorporation of the Asp inside the liposomal nanovesicles was studied using a dual-beam spectrophotometer (Peak instruments T-9200, USA).

2.8.2. Stability in physiological conditions. The stability of Asp/TLs was studied in a cell culture medium to simulate the physiological conditions, as previously described with some modifications.[33] In brief, 150 μL of Asp/TLs was mixed with 850 μL DMEM medium fortified with FBS (10%), and then incubated for 24 h at 37 °C. Afterward, aliquots of the Asp/TLs formulation were withdrawn at various intervals to study the size, PDI, and EE% to test the stability of the prepared formulation.

2.8.3. *In vitro* temperature-dependent release study of Asp. The % Asp release was performed at different temperatures (37, 38, 39, and 40 °C) to investigate the hyperthermia effect on the % drug released. In brief, a specific amount of Asp/TLs were loaded into a dialysis sack (MWCO = 12 − 14 k_D) and incubated in 15 mL of phosphate buffer saline (pH 7.4) supplemented with 1.5% tween 80 pre-heated to the temperatures mentioned above while stirring at 150 rpm. A 1 mL aliquot of the release medium was withdrawn at different intervals (ranging from 0 to 60 min). Sink conditions were maintained by immediately adding an equal volume of fresh pre-heated buffer solution to replace the withdrawn release medium. The Asp concentration was quantified spectrophotometrically at 283 nm using a dual-beam spectrophotometer (Peak Instruments T-9200, USA). The amount of Asp released was determined using eqn (2) shown below.

$$\text{Asp release } (\%) = \frac{\text{Asp released}}{\text{Initial amount of Asp}} \times 100 \quad (2)$$

2.8.4. Cell culture. The MDAMB 231 cell line was obtained from the American Type Culture Collection (ATCC, Wesel, Germany), grown in Dulbecco's modified Eagle's medium DMEM with 10% fetal bovine serum, 1% antibiotic-antimycotic and L-glutamine, and incubated at 37 °C under 5% CO_2 and standard culture conditions.[34] Trypsinization was performed upon reaching 80–90% cell confluence.

2.8.5. Cellular viability. A modified 3-(4,5-dimethylthiazol-2-yl)-2,5-diphenyl-tetrazolium bromide (MTT) assay was used to evaluate the cell viability as performed elsewhere.[35] Briefly, 10 000 cells were cultured with 100 μL medium in each well of the 96-well plates. The plates were incubated at 37 °C under 5% CO_2 (standard culture conditions) for 24 h. Then, cells were treated with ten different concentrations (0.01, 0.03, 0.1, 0.3, 1, 3, 10, 30, 100, and 300 μg mL^{-1}) of the six investigated substances. One of the culture plates that contained cells treated with Asp and Asp/TLs was incubated for 3 h at 37 °C, then for 1 h at 40 °C (thermal treatment). This was followed by incubation at 37 °C for 48 h. Another culture plate that contained cells treated with Asp, TLs, and Asp/TLs was placed directly at 37 °C for 48 h without exposure to any thermal treatment. There was no change in the culture medium during the treatment period, so the test agent stayed in contact with the cells for 48 h duration. Test compounds were added to wells containing medium alone as a blank to avoid any interference with the colorimetric MTT assay. After 48 h, 16 μL of 5 mg mL^{-1} MTT was added to each well, and plates were incubated for 3.5 h. The growth medium was then discarded, and 120 μL of dimethyl sulfoxide was added, followed by 15 min shaking using the orbital shaker. Absorbance was measured at 490 nm. The assay was done in triplicate for each concentration of the tested substances.

2.8.6. Apoptosis assay. Apoptosis assay was performed to detect the apoptotic and necrotic cell populations after exposure to the test samples. The assay was based on the utilization of Annexin V-FITC apoptosis detection kit (Abcam Inc., Cambridge Science Park, Cambridge, UK), as per the manufacturer's guidelines. Cells were incubated at 37 °C under 5% CO_2 for 24 h. On the following day, cells were exposed to Asp (40 °C) and Asp/TLs (40 °C) treatments for 3 h at 37 °C, then for 1 h only at 40 °C (thermal treatment). Cells were then kept at 37 °C again for 48 h. Thereafter, 100 000 cells were harvested by trypsinization and washed with ice-cold PBS. Cells were then mixed with Annexin V-FITC/PI solution and left in the dark at room temperature for half an hour. Lastly, the stained cells were analyzed using ACEA 2 fluorescent channels Novocyte™ flow

Table 2 List of primers used in the RT-qPCR

Primer ID	Primer sequence (5′ – 3′)	Company
β-actin F	CACCATTGGCAATGAGCGGTTC	Metabion International AG
β-actin R	AGGTCTTTGCGGATGTCCACGT	
Bax F	TCAGGATGCGTCCACCAAGAAG	
Bax R	TGTGTCCACGGCGGCAATCATC	
BAK F	CGACATCAACCGACGCTATG	
BAK R	CCACTCTCAAACAGGCTGGTG	
BCL-xL F	GAAAGCGTAGACAAGGAGATG	
BCL-xL R	AAGAGTGAGCCCAGCAGAA	
BCL-2 F	ATCGCCCTGTGGATGACTGAGT	
BCL-2 R	GCCAGGAGAAATCAAACAGAGGC	
P53 F	CCTCAGCATCTTATCCGAGTGG	
P53 R	TGGATGGTGGTACAGTCAGAGC	

cytometer (ACEA Biosciences Inc., San Diego, CA, USA), and quadrant analysis was performed as described previously.[36]

2.8.7. Gene expression analysis. Total cellular RNAs were isolated from cells using the QIA amp Viral RNA Mini Kit (Qiagen, Hilden, Germany). The extracted RNAs were then reverse transcribed into cDNA using the ReverAid RT Kit (ThermoFisher Scientific, Waltham, USA) and Bio-Rad™ 100 thermal cycler. All steps were performed as per the guidelines provided by the kits' manufacturers. An estimate of 1 μL of cDNA was collected from each sample to be further assayed by quantitative real-time PCR for the target genes and β-actin (housekeeping gene). The primers used in the RT-qPCR are clearly described in Table 2. The assay was completed on a Rotor-Gene Q-Qiagen Real-time PCR thermal cycler. The obtained data were normalized to β-actin, and the relative normalized gene expression values were calculated by the $2^{-\Delta\Delta C_t}$ method.[37]

2.8.8. Statistical analysis. GraphPad Prism 6 was used for data analysis. The results are the average of triplicates ± standard deviation (SD). ANOVA was used to compare the three groups. This was followed by multiple-comparison post hoc tests to determine the significance among every two groups. The non-parametrical Kruskal–Wallis and Mann–Whitney tests were used whenever the data deviated from the normal distribution. Statistical significance was considered at p-value ≤ 0.05.

3. Results and discussion

3.1. Optimization using three-factor, three-level Box–Behnken response surface design (3^3BBD)

Optimizing the preparation conditions of the liposomal formulations is crucial in improving the physicochemical properties of the liposomes and their ability to deliver their cargo to the intended site of therapeutic actions.[38] In this regard, a three-factor, three-level Box–Behnken response surface design (3^3BBD) was performed for formulation optimization. The responses of particle size (PS, Y1), zeta potential (ZP, Y2), polydispersity index (PDI, Y3), and entrapment efficiency (EE%, Y4) were fitted individually to quadratic models for reaching the best model to use with the highest adjusted and prediction R^2 (all adjusted $R^2 \geq 0.9$). Non-significant model terms were eliminated to reach higher R^2. As shown in Table 3, the quadratic model was selected for all four responses. Analysis of variance (ANOVA) testing of the obtained results was performed at a p-value <0.05. After model reduction, the final equations related to different factors and interactions for the responses were created *via* Design-Expert Version 12.0.1.0 (Stat-Ease Inc., Suite 480, Minneapolis, MN, USA) in terms of coded variables.

The four equations were as follows:

$$\mathrm{PS} = 136.34 + 30.37A + 0.50B + 7.01C + 2.25AB + 0.18AC - 7.36BC + 14.06A^2 - 0.31B^2 + 1.38C^2$$

$$\mathrm{PDI} = 0.25 + 0.08A - 0.004B - 0.003C - 0.004AB - 0.003AC + 0.007BC - 0.04A^2 + 0.006B^2 - 0.002C^2$$

$$\mathrm{ZP} = -31.65 + 6.83A + 0.66B + 0.35C - 1.08AB + 1.21AC - 0.30BC + 13.45A^2 + 3.67B^2 + 4.66C^2$$

$$\mathrm{EE\%} = 84.83 - 8.85A + 0.28B + 0.22C - 1.57AB + 0.43AC - 0.54BC - 13.20A^2 + 0.10B^2 - 1.12C^2$$

3.1.1. Influence of the independent factors: particle size (PS). Nano-scale particle size is a key player that is essential in improving therapeutic efficiency by boosting cellar uptake *via* enhancing the diffusion across cell membranes *via* enhanced retention and permeability effect (EPR).[39] All of the prepared Asp/MLs formulae had small PS ranging from 119 to 185 nm, as presented in Table S1.† Thus, the constraint criterion of PS was set as "in range", in the optimization part of the study, as presented in Table 3. ANOVA analysis revealed that factors A (cholesterol : 2 DPPC molar ratio) and C (lipids : drug molar ratio) significantly affected PS, with $p < 0.0001$ and $p = 0.01$, respectively. Fig. 2A illustrates that increasing factors A and C, in the tested limits led to a significant increase in particle size. The direct relationship between the cholesterol : 2 DPPC molar ratio and the size of the liposomes may be attributed to the interactions between lipid chains of phospholipids and the added cholesterol, causing an increase in inter-lipid space and leading to membrane thickness expansion.[40,41] Another underlying cause of this relationship was that, at high concentrations, cholesterol increases interactions in the hydrophobic bilayers, thus strengthening the packing of bilayers, resulting in reduced fluidity and larger liposomal size.[42] Moreover, the directly proportional relationship between the same response and the lipids; drug molar ratio may be due to the accumulation of lipids in the hydrophobic part of the membrane affecting the interactions between the acyl chains of phospholipids and inducing swelling of the membrane, leading to the formation of larger vesicles.[43] In addition, the increased PS detected by Dynamic Light Scattering (DLS) may be attributed to liposomal aggregation at higher lipid concentrations.[38] Nonsignificant interaction was detected between factors A and C. On the other hand, a significant interaction was found between DSPE-PEG 2000 : 2 DPPC molar ratio and lipids : drug molar ratio ($p < 0.05$), as depicted in Fig. 2B. It was observed that

Table 3 Model summary statistics of the various models for the investigated responses, constraints for optimization of Asp/TLs preparations, and the predicted and observed values of the responses

Response		Model	R^2	Adjusted R^2	Predicted R^2	Constraint	Predicted mean	Observed mean	95% Prediction Interval
Y1	Particle size (nm)	Quadratic	0.97	0.94	0.60	In range	119.87	114.05 ± 1.56	102.26–137.49
Y2	Polydispersity index	Quadratic	0.99	0.98	0.97	Minimize	0.13	0.15 ± 0.015	0.10–016
Y3	Zeta potential (mV)	Quadratic	0.98	0.96	0.93	Maximize	−13.80	−15.24 ± 0.65	(−19.87)–(−7.74)
Y4	Entrapment efficiency (%)	Quadratic	0.98	0.94	0.91	Maximize	82.05	84.08 ± 2.75	75.18–88.92

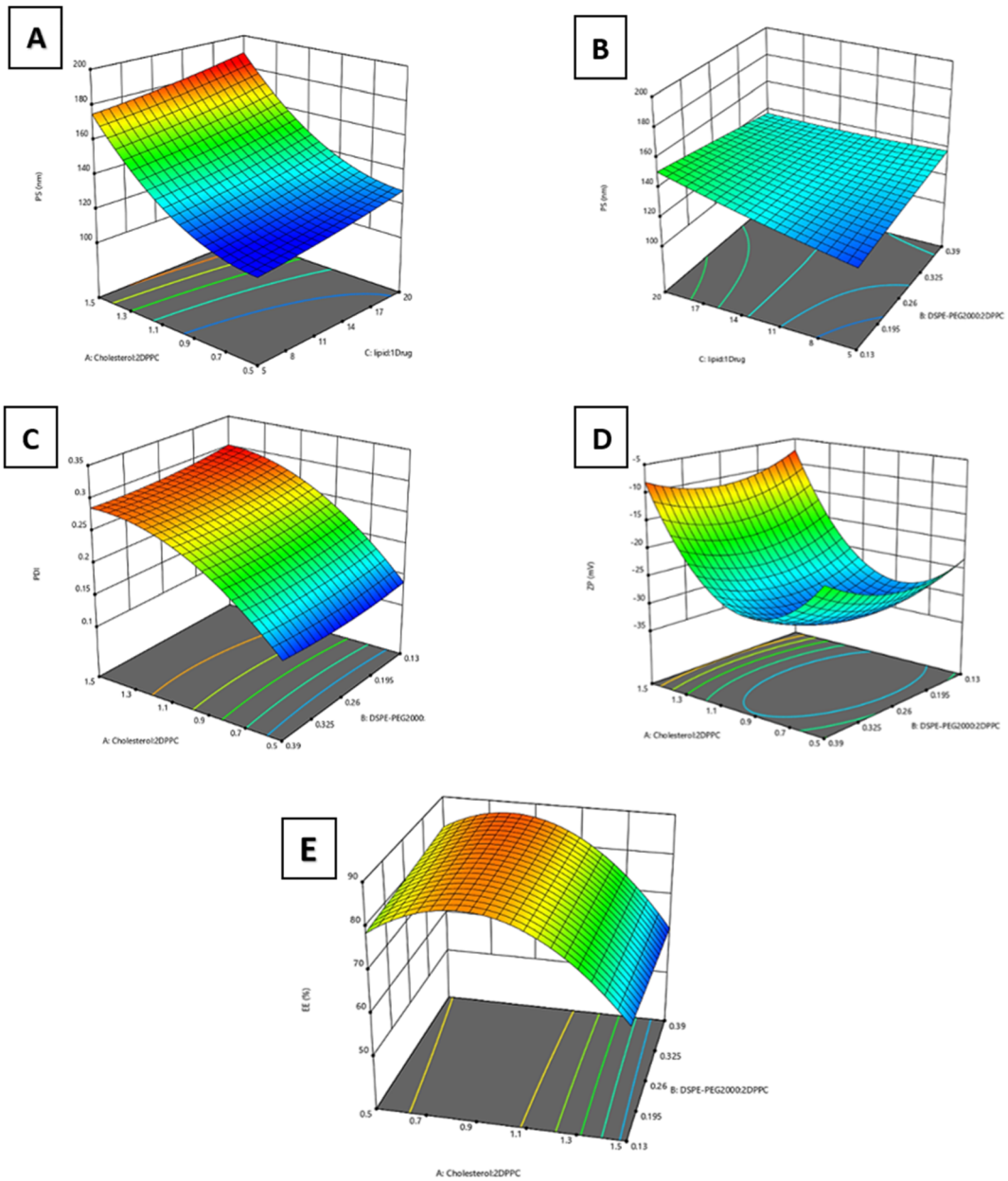

Fig. 2 Three-dimensional surface plots for the main effects and interactions of the independent factors of Asp/TLs formulae (cholesterol : 2 DPPC molar ratio, DSPE-PEG 2000 : 2 DPPC molar ratio, and lipids : drug molar ratio) on PS (A and B), PDI (C), ZP (D), and EE% (E).

increasing the DSPE-PEG 2000 : 2 DPPC molar ratio leads to a diminishing effect of the lipids : drug molar ratio on PS. This was attributed to the steric stabilization of liposomes achieved by the presence of the PEG polymer, which prevents the aggregation of liposomes and enhances their stability. PEG has bulky polymeric chains that offer higher steric hindrance. This favors high surface curvature and/or micellar structure, which was reported to favor the formation of bilayer discs.[38]

3.1.2. Influence of the independent factors: PDI. PDI was considered in this study because it indicates the uniformity of the prepared liposomes. ANOVA analysis showed that PDI was significantly affected by only factor *A* (cholesterol : 2 DPPC molar ratio), with $p < 0.0001$ (Fig. 2C). Our findings are in line with previous studies that reported the effect of increasing cholesterol concentration on increasing the polydispersity of the prepared nanovesicles.[38,40,42] Nonsignificant interaction was detected between factor *A* and the other two factors (*B* and *C*), as presented in Fig. 2C. It was revealed that increasing the initial lipid concentration was shown to increase the liposomal size without significantly affecting the nanoparticles' dispersity.[17]

3.1.3. Influence of the independent factors: ZP. High absolute zeta potential values suggested the high stability of the prepared liposomes and their prolonged shelf-life time. ANOVA analysis showed that only factor *A* (cholesterol : 2 DPPC molar ratio) significantly affected the surface charge, with $p < 0.0001$. It was found that increasing the cholesterol : 2 DPPC molar ratio up to 0.85 : 2 increased the negative charge of the Asp/TLs. As the cholesterol units increase, the negatively charged DPPC units will increase within the liposomal bilayer, leading to an increase in PS, as previously mentioned, and in negative charge.[42] Conversely, increasing the cholesterol : 2 DPPC molar ratio beyond 0.85 : 2 has significantly diminished the liposomal negative charge. This is attributed to replacing the negatively charged phospholipids with neutral cholesterol, affecting the overall charge of each nanoparticle.[35] Similarly, no significant interaction was detected between factor *A* and any of the other two factors, as presented in Fig. 2D.

3.1.4. Influence of the independent factors: entrapment efficiency (EE%). ANOVA analysis of the liposomal EE% showed that only factor *A* (cholesterol : 2 DPPC molar ratio) significantly affected drug entrapment, with $p < 0.0001$. The behavior of EE% with increasing cholesterol levels was precisely the reverse of the ZP pattern previously explained. It was noted that upon increasing the cholesterol; 2 DPPC molar ratio up to 0.85 : 2, the

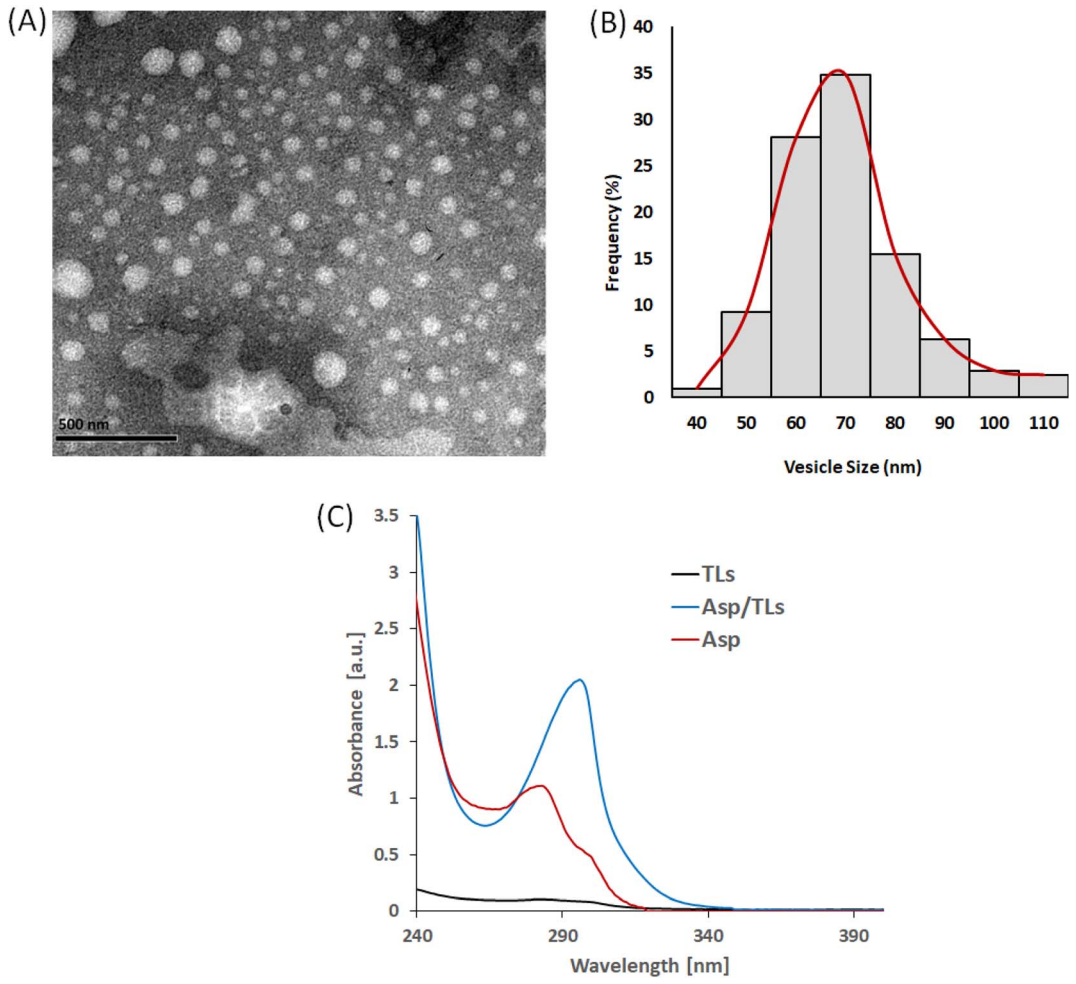

Fig. 3 (A) TEM image of the optimal Asp/TLs, (B) vesicle (nm) histogram of the optimal Asp/TLs formulation, generated utilizing the image processing program Image J (NIH, Bethesda, MD, USA), and (C) UV spectra of void TLs, Asp/TLs, and free Asp.

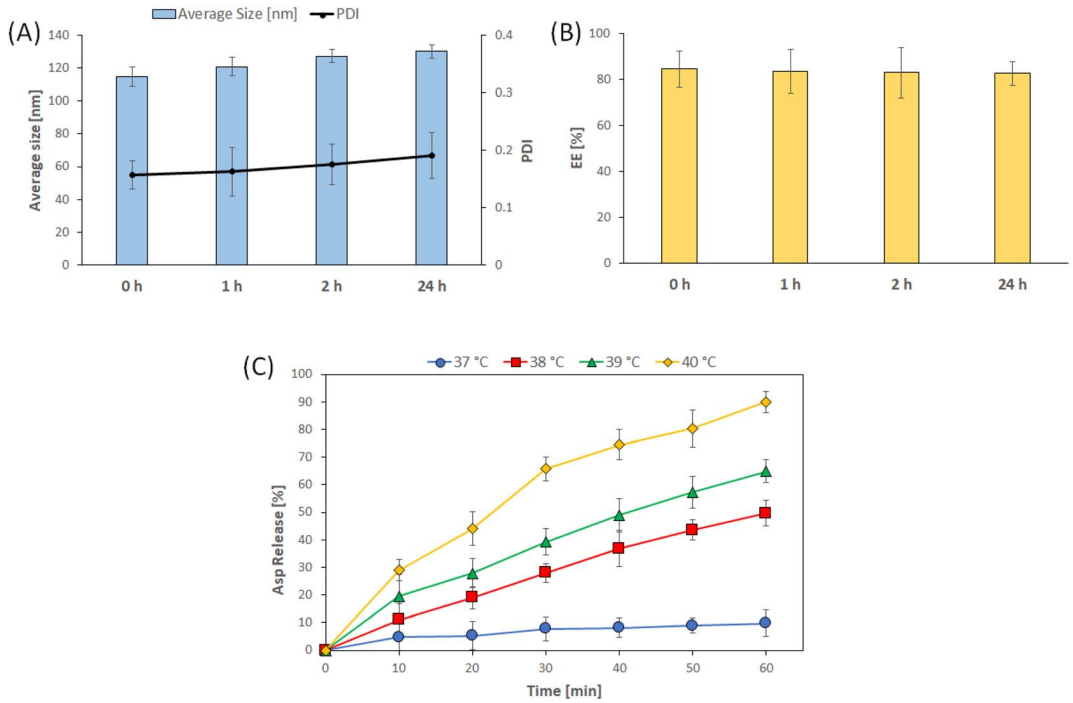

Fig. 4 Serum stability of Asp/TLs incubated in DMEM and FBS (10%) in terms of (A) average size and PDI, and (B) EE%. (C) Temperature-triggered release of Asp from Asp/TLs at different temperatures (37, 38, 39, 40 °C). All findings are expressed as mean ± SD of three independent experiments.

EE% was increased. However, when increasing the cholesterol; 2 DPPC molar ratio above 0.85 : 2, the EE% was significantly decreased beyond this ratio, as presented in Fig. 2E. This might be attributed to the electrostatic interactions between the positively charged platinum-based drug (Asp) and the negatively charged liposomes, which led to high entrapment efficiencies.[44] Interactions between factor *A* and the other two factors were insignificant, as presented in Fig. 2E.

3.2. Characterization of the optimized Asp/TLs

Design-Expert 12® software (Stat-Ease Inc., Minneapolis, MN, USA) was used to select the optimized formulation, with an overall desirability of 0.813, after applying PS, PDI, ZP, and EE % constraints (shown in Table 3). Since all of the obtained particle sizes were in an acceptable range (119–185 nm), the particle size constraint was kept "in range". Regarding the remaining responses, the constraints applied to the PDI, ZP, and EE% were "minimized", "maximized", and "maximized", respectively. The suggested that the optimal Asp/MLs preparation was then formulated and characterized, and the observed means of PS, PDI, ZP, and EE% ($n = 3$) fell inside the 95% two-sided prediction confidence interval ($\alpha = 0.05$), which validated the optimization procedure performed.

Table 4 Cytotoxicity of samples against triple-negative breast cancer (MDA-MB231)[a]

Sample	IC_{50} on MDA-MB231 cell line # (μg mL^{-1})
Asp	6.6 ± 0.34
TLs	>300
Asp (40 °C)[b]	3.83 ± 0.18
Asp/TLs	186 ± 4.83
Asp/TLs (40 °C)[b]	0.9 ± 0.03

[a] IC_{50} values are the mean of triplicate experimental runs ± standard deviation. [b] The two samples with the lowest IC_{50} values are the most potent on MDA-MB-231.

3.2.1. Morphological features and UV-vis analysis. Transmission electron microscopy (TEM) analysis was carried out to evaluate the morphology of the prepared Asp/TLs vesicles and detect their average particle size. The prepared Asp/TLs exhibited a spherical shape and smooth surfaces with no apparent aggregations (Fig. 3A). In addition, TEM analysis revealed the uniformity of the prepared nanovesicles. Moreover, the average vesicles' size was measured using the Image J software (NIH, Bethesda, MD, USA), and was found to be 64.64 ± 12.98 nm (Fig. 3B). This size was smaller than that measured by the Zetasizer (114.05 ± 1.56 nm). The higher particle size detected by the DLS technique could be attributed to the Brownian motion exerted by the suspended small Asp/TLs particles.[45] Also, this larger size was because the zeta sizer measured the particles' hydraulic diameter, including the thickness of the water boundary layer surrounding the particles.[46]

The loading of Asp into thermosensitive liposomes was revealed to cause a red shift to a longer wavelength, from 283 nm in the case of Asp to 297 nm in the case of Asp/TLs. This red shift in the Asp spectrum clearly indicated the successful entrapment of the platinum drug into the TLs.[47]

3.2.2. Stability of the optimal Asp/TLs under physiological conditions. Since the liposomal size, uniformity, and drug leakage assessment are vital in developing an optimal formulation to deliver chemotherapeutics effectively, we evaluated the integrity of the prepared optimal Asp/TLs under physiological conditions. In this regard, Asp/TLs were incubated with DMEM medium fortified with FBS (10%) to simulate the conditions of the cell culture assays, and the average size, PDI, and EE% were investigated after 0, 1, 4, and 24 h.[48] As shown in Fig. 4A, a trivial increase in the size and PDI and a minimal decrease in the EE% of the vesicles was observed throughout the 24 h (duration of the study), as presented in Fig. 4A and B. The stability of the prepared Asp/TLs under physiological conditions was attributed to the steric repulsion caused by the PEG present in the liposome components. This discourages the opsonization phenomenon (the adsorption of proteins on the liposomal bilayers) and hence minimizes the altering of the physicochemical properties of the liposomes by the protein corona.[49,50] The opsonization phenomenon is responsible for the premature diffusion of the loaded drugs out of the thermo-responsive liposomal lipid bilayers at the physiological body temperature.[51] Thus, our findings indicated the stability of the prepared Asp/TLs at 37 °C, which prevented the premature leakage of the loaded Asp in the circulation before reaching the intended site of action. Our findings aligned very well with previous studies that reported the stability of PEGylated liposomes under physiological conditions.[33,52]

3.2.3. *In vitro* temperature-dependent release study of Asp. To confirm the successful release of Asp from the optimized smart thermo-responsive liposomes upon heat trigger, a release study was carried out at different temperatures (37, 38, 39, and 40 °C), as illustrated in Fig. 4C. The lipid phase transition temperature (T_m) at 37 °C showed that only 9.5% of Asp was released within 60 min from the TLs optimized formulation. An increase in Asp release % from TLs was observed within 60 min after increasing the temperature, in which 49.7%, 64.8%, and 90% of Asp were increased upon raising the temperature to 38, 39, and 40 °C, respectively. Increasing the Asp release % was attributed to the local hyperthermia effect, which enhanced the disassembly of the liposomal lipid bilayer *via* enhancing the phase transition temperature-dependent transformation from the solid gel phase to the liquid one. This increased the lipid

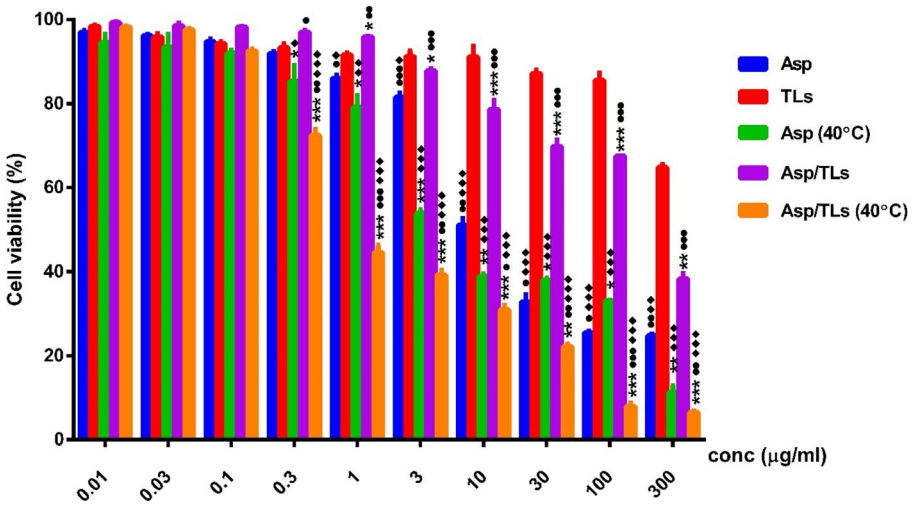

Fig. 5 Cell viability of MDA-MB-231 cells after treatment with the test compounds at 10 different concentrations for 48 h. Both Asp (40 °C) and Asp/TLs (40 °C), (*i.e.*, cells exposed to 1 h of thermal treatment) demonstrated the lowest IC_{50}s, and proved to be the most potent among all treatment options. Data represent the mean ± standard deviation of triplicate experiments. The symbols (*), (●) and (◆) refer to statistical significance from Asp, Asp (40 °C), and Asp/TLs, respectively. The existence of any symbol once only indicates significance with *P*-value ≤0.05. Any duplicated symbol indicates significance with *P*-value ≤0.01, and any symbol that is presented as triplicate indicates *P*-value ≤0.001.

Table 5 Apoptosis assay of MDAMB-231 cells after treatment with Asp (40 °C) and Asp/TLs (40 °C) for 48 h[a]

	Percent cell population		
Apoptotic stage	Control	Asp (40 °C)	Asp/TLs (40 °C)
Necrosis (Q2-1)	0.5 ± 0.03	***39.37 ± 0.58	●●● *** 48.08 ± 0.15
Late apoptosis (Q2-2)	0.7 ± 0.09	***10.91 ± 0.61	●●● *** 23.34 ± 0.16
Early apoptosis (Q2-4)	0.19 ± 0.09	0.07 ± 0.01	0.33 ± 0.05
Viable cells (Q2-3)	98.6 ± 0.23	***49.65 ± 1.15	●●● *** 28.24 ± 0.3

[a] The provided percent is the mean of triplicate independent runs ± standard deviation. *** Indicates high significance from the control (untreated) where *P*-values ≤0.001. ● ● ● Indicates high significance from Asp (40 °C) where *P*-values ≤0.001.

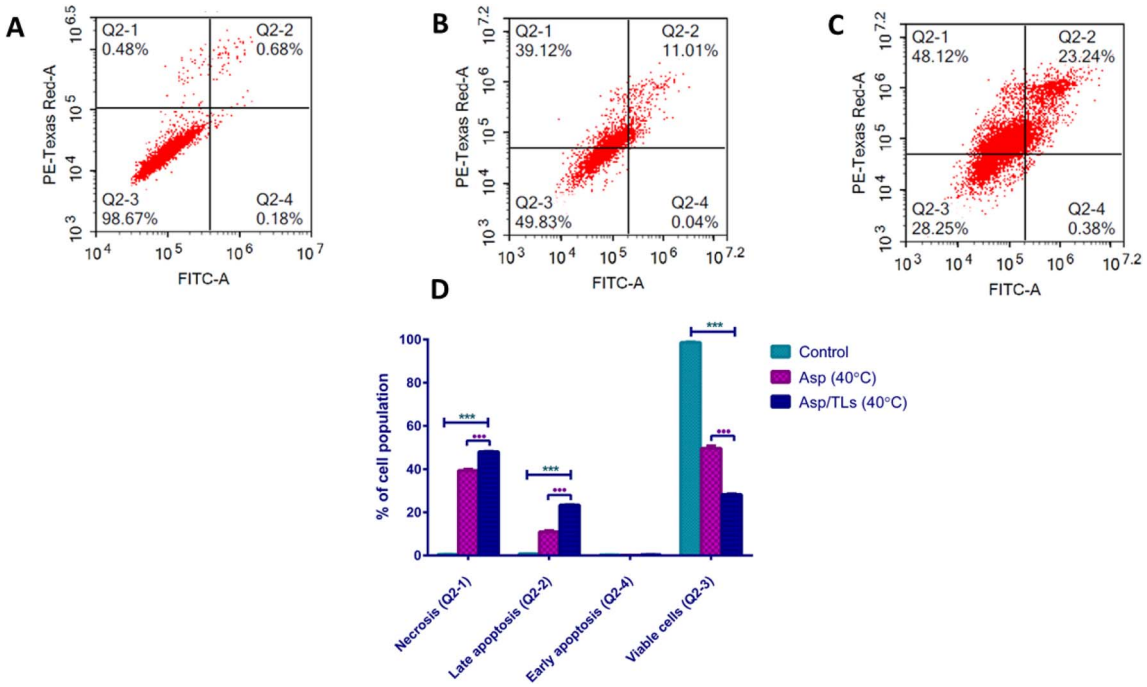

Fig. 6 Apoptosis in MDA-MB-231 cells after 48 h exposure to Asp (40 °C) and Asp/TLs (40 °C). Cytograms presenting annexin-V/propidium iodide-stained untreated MDA-MB231 cells as negative control (A), cells treated with Asp (40 °C) (B), cells treated with Asp/TLs (40 °C) (C), and representation of the apoptosis analysis results (D). Quadrant charts show Q2-1 (necrotic cells, AV−/PI+), Q2-2 (late apoptotic cells, AV+/PI+), Q2-3 (normal cells, AV−/PI−), Q2-4 (early apoptotic cells, AV+/PI−). Data represented are the average triplicate experimental trials ± standard deviation (SD). ***Refers to high significance from the control where p-values ≤0.001. ● ● ● Refers to a significant deviation from Asp (40 °C) where P-values ≤0.001.

bilayer's permeability, triggering the thermal-dependent diffusion of Asp out of the TLs.[24,32] Our findings were in line with a previous study by Gaber *et al.*, who reported the ability of TLs to release around 40% of their cargo after heat treatment for 30 min.[51] The release study findings can be considered a proof-of-concept of the ability of the optimized TLs system to release their cargo, Asp, preferentially in cancer cells upon being triggered by local hyperthermia.

3.2.4. Cell viability (MTT assay). MDA-MB-231 cells were exposed to ten varying concentrations (ranging from 0.01 to 300 μg mL^{-1}) of the six investigated samples for 48 h. Two of the investigated samples, free Asp (40 °C) and the optimal Asp/TLs (40 °C) received thermal treatment at 40 °C for 1 h only during the whole process. The MTT assay was utilized to detect cell viability after exposure to all test compounds. The results are clearly displayed by Table 4 and Fig. 5. Void liposomes were deployed as vehicle control and reported an IC_{50} > 300 (*i.e.*, no observable effect on cell viability). Therefore, the void liposomes displayed a good safety profile and showed no toxicity when applied to the cells.

Recent research has pointed to the advantages of introducing mild hyperthermia along with chemotherapy.[53] Interestingly, the two samples exposed to mild thermal treatment, Asp (40 °C) and Asp/TLs (40 °C) reported the lowest IC_{50} values of 3.83 and 0.9 μg mL^{-1}, respectively, as shown in Table 4 and Fig. 5. Accordingly, exposure to mild hyperthermia for 1 h resulted in a remarkable improvement in the cytotoxic activity of the free drug, as well as that loaded onto liposomes. This could be explained in terms of the ability of mild hyperthermia to increase tissue perfusion and permeability, leading to better drug delivery and maximized drug effectiveness at the tumor cells.[53]

Our findings showed that at normal physiological temperature (37 °C), the free Asp possessed much higher cytotoxic activity (IC_{50} = 6.6 μg mL^{-1}) than Asp/TLs (IC_{50} = 186 μg mL^{-1}). This indicates that the drug content remained entrapped within the thermosensitive liposomes at 37 °C, and was released only upon exposure to a temperature of 40 °C for a short period (1 h). Likewise, a former study showed that the chemotherapeutic drugs nedaplatin and picoplatin stayed within thermosensitive liposomes at 37 °C, and exerted their cytotoxic activity only when exposed to a mild increase in temperature (40 °C). Researchers attributed this to the release of drug content above the T_m of the lipids from which such liposomes were synthesized.[32] The lipid bilayer has been noted to change from a solid gel assembled phase to a liquid disassembled phase at this temperature (40 °C), which would definitely enhance the permeability and fluidity of the liposomal lipid bilayer.[54] As a result, the TLs loaded with either hydrophilic or hydrophobic molecules should be released when the temperature is increased to 40 °C. These results were consistent with an earlier study, which showed that TLs could release more than 40% of its content in half an hour at 40 °C.[24]

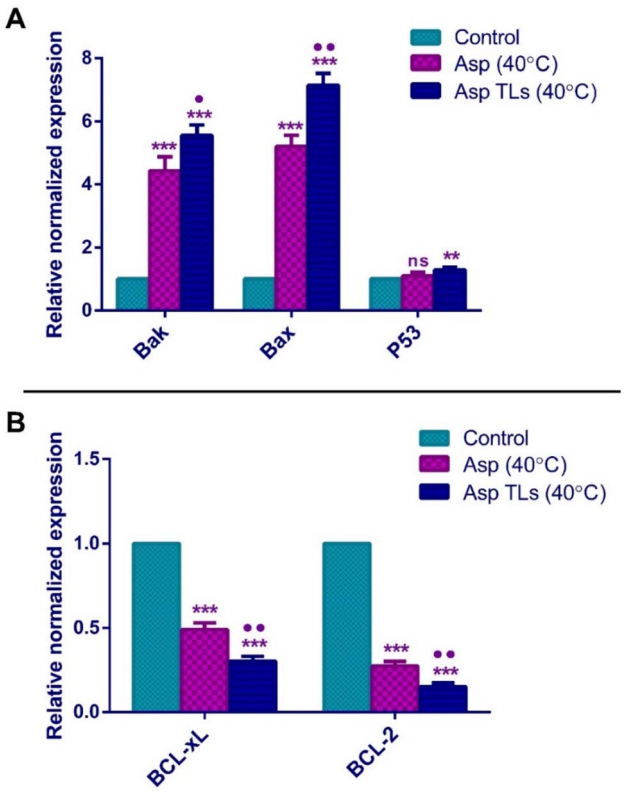

Fig. 7 RT-qPCR analysis of the relative normalized gene expression of the apoptotic genes (A) and the antiapoptotic genes (B). All data were normalized to control (untreated cells), and β-actin was deployed as a housekeeping gene. ***Refers to high significance from the control where *p*-values ≤0.001. **Indicates significant difference from the control where *p*-values ≤0.01. ● Means significant deviation from Asp (40 °C) where *P*-values ≤0.05. ● ● Refers to significant deviation from Asp (40 °C) where *P*-values ≤0.01. ns stands for nonsignificant.

Long-circulating nanoparticles are retained significantly in tumors due to the lack of a functioning lymphatic system in these tissues, which makes it difficult for nanoparticles to be cleared effectively.[55] The enhanced permeability and retention (EPR) phenomenon is crucial in liposomal drug delivery. This partly explained the reduced off-site toxicity and the approval of many liposomal formulations for clinical use.[56] Since it relied on passive drug diffusion across the liposomal lipid bilayer, it has been noted that drug release from the liposomal carrier is sometimes delayed and might lower the peak concentrations.[57] Accordingly, a different strategy in which the drug is entrapped in the aqueous core of TLs might lead to a medication with better pharmacokinetic properties.[58] Exposure to mild hyperthermia (40–43 °C) triggered the liposomes to discharge their payload rapidly. Numerous preclinical and clinical research studies have examined the effects of heating the targeted tissue to these temperatures, such as with radiofrequency or high-intensity focused ultrasound, leading to fast intravascular release and considerable drug accumulation in the tumor site.[59–62]

In this study, Asp loaded into liposomes and exposed to mild hyperthermia (Asp/TLs (40 °C)) possessed the most potent cytotoxic activity among all the investigated substances. The optimal Asp/TLs (40 °C) recorded an IC_{50} of 0.9 μg mL^{-1}, while the free drug Asp at 37 °C and at 40 °C recorded IC_{50} values of 6.6 and 3.83 μg mL^{-1}, respectively. The hybrid system, Asp/TLs (40 °C), increased the cytotoxicity of Asp (40 °C) by approximately 4-fold, suggesting an important role for TLs in increasing the anticancer activity of the free drug, Asp. Our findings proved that incorporating Asp into TLs helped decrease the required drug dose and improve its therapeutic index. This was in line with a study performed by Alawak *et al.*, who showed that TLs augmented the chemotherapeutic effect of doxorubicin and reduced the required dose to minimize its side effects.[63]

3.2.5. Apoptosis assay. MDA-MB-231 cancer cells were treated with the two most potent compounds, Asp (40 °C) and Asp/TLs (40 °C). The results are presented in Table 5 and Fig. 6. Treatment with free Asp (40 °C) resulted in a 15-fold increase in the late apoptosis profile compared to the control (non-treated cells). As described, Asp is a prodrug comprising both aspirin and cisplatin. A previous research study has shown a remarkable increase in the apoptotic effects of cisplatin when combined with aspirin.[11] Herein, treatment with Asp (40 °C) also resulted in about a 50% reduction in the viable cell population relative to the untreated MDA-MB-231 cells (control).

Exposure to mild hyperthermia has been associated with cytotoxicity to tumor cells, improved chemosensitivity, and enhanced particle extravasation from the vasculature into the tumor microenvironment.[64] As expected, the optimal Asp/TLs (40 °C) caused an impressive increase in the percentage of cell population among both the late apoptosis and necrosis quartiles (denoted by *P*-value ≤0.001) when compared to the free drug, Asp (40 °C). Furthermore, exposure to the optimal Asp/TLs (40 °C) resulted in a 72% reduction in the viable cells compared to the control, and about a two-fold decrease in viable cells to free Asp (40 °C). As such, the optimal Asp/TLs (40 °C) significantly induced apoptosis and necrosis, and reduced the viable cells more than free Asp (40 °C), (*P*-values ≤0.001).

3.2.6. Molecular analysis of several apoptotic and anti-apoptotic genes. RT-qPCR was used to evaluate the relative normalized gene expression of several biomarkers in the molecular apoptosis pathway in MDA-MB-231 cells after exposure to the test samples for 48 h. RT-qPCR was performed on the apoptotic genes; *Bak*, *Bax*, and *P53*, as well as the anti-apoptotic genes; *BCL-xL* and *BCL-2*, to provide further evidence for the apoptosis assay on the molecular level.

The pro-apoptotic *Bcl-2* family members, *Bak* and *Bax*, are essential genes for apoptosis. *Bak* and *Bax* usually oligomerize upon activation and translocate to the outer membrane of the mitochondria, where they perforate the mitochondrial membrane and induce the release of cytochrome c into the cytosol. This ultimately causes cell death by triggering the caspases' cascade.[65] The overexpression of *Bak* gene has been noted to sensitize cancer cells to the apoptotic effects of chemotherapy. Meanwhile, the reduced *Bak* levels were associated with poor prognosis and failure to respond to the chemotherapeutic drugs. The downregulation of the *Bax* gene has also been associated with resistance to chemotherapy and poor prognosis in several tumors, including breast and ovarian cancers.[66,67] In the current

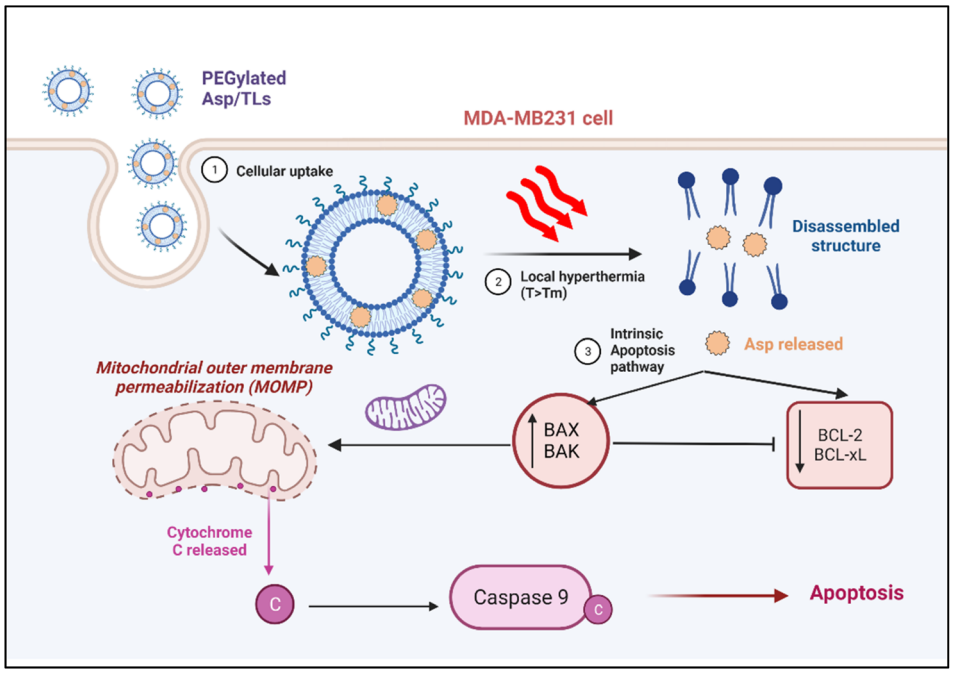

Fig. 8 Molecular mechanism of optimal Asp/TLs in triple negative breast cancer: the mechanism by which the optimal Asp/TLs induce apoptosis in the invasive triple-negative breast cancer cells, MDA-MB-231.

study, Asp (40 °C) treatment of MDA-MB-231 breast cancer cells resulted in a 4.4-fold and 5.2-fold increase in the expression of *Bak* and *Bax*, respectively. Likewise, the overexpression of *Bak* and *Bax* in response to Asp has been previously noted in cervical (HeLa) and liver (HepG2) cancer cells.[11] The optimal Asp TLs (40 °C) caused a 5.6-fold and 7.2-fold increase in the expression of Bak and Bax, respectively. As shown in Fig. 7A, Asp TLs (40 °C) resulted in a significantly higher expression of both pro-apoptotic genes *Bak* and *Bax* as compared to free Asp (40 °C). As such, it was suggested that the optimal Asp TLs (40 °C) possess amplified apoptotic effects on the molecular level, where it caused a remarkable increase in *Bak* and *Bax* levels, thereby providing further evidence for their apoptotic effects and favoring the apoptotic effects of the chemotherapeutic drug, asplatin (Fig. 8).

The tumor suppressor gene, *P53*, has demonstrated a complicated involvement in the carcinogenesis process since both gain and loss of its function mutations have been observed among different tumors.[68] In general, *P53* was found to trigger the expression of pro-apoptotic genes like *BAX* and *PUMA*, thus promoting apoptosis.[69] The free Asp (40 °C) did not induce any significant difference in *P53* expression when compared to the untreated cells (control) (Fig. 7A). Similar findings were reported in a previous study in which Asp did not exhibit any significant effect on *P53* gene expression in cervical (HeLa) and liver (HepG2) cancer cells.[11] Surprisingly, the optimal Asp TLs (40 °C) caused a significant increase (about 1.3-fold) in *P53* gene expression relative to the control cells. Therefore, Asp TLs (40 °C) showed additional activity by inducing the tumor suppressor, *P53*, which provided an added clue to its enhanced apoptotic effects.

BCL-2 is an anti-apoptotic protein that promotes cell survival. It was first identified in B-cell lymphomas (non-Hodgkin's lymphoma), then in various tumors. The upregulation of *BCL-2* genes usually interferes with chemotherapy, and leads to unfavorable prognosis in cancer patients.[70] *BCL-xL* is a homolog of *BCL-2* that counteracts the apoptotic effects of chemotherapeutic agents and hinders cellular response to therapy. *BCL-xL* prevents apoptosis by binding to the pro-apoptotic proteins like *BAX* and *BAK*, thereby inhibiting their apoptotic activity.[71,72] Various cancers, including B-cell lymphomas and breast and prostate cancers, are affected by the overexpression of *BCL-2* and *BCL-xL*, allowing cancer cells to avoid programmed cell death.[73] The free Asp (40 °C) treatment significantly reduced the normalized gene expression of the anti-apoptotic markers, *BCL-xL* and *BCl-2*, by 50% and 73%, respectively (Fig. 7B). The optimal Asp TLs (40 °C) treatment showed a more pronounced decrease in *BCL-xL* and *BCl-2* gene expression as compared to that of Asp (40 °C). Asp TLs (40 °C) lowered the expression levels of both *BCL-xL* and *BCl-2* by 70% and 85%, respectively (Fig. 7B).

In summary, exposure to mild hyperthermia stimulated the uptake of Asp TLs by breast cancer cells, and promoted the release of their drug content in the tumor microenvironment. The released Asp was shown to exert its cytotoxic activity by activating the intrinsic pathway of apoptosis, whereby it caused a significant increase in the expression of the apoptotic proteins Bak and Bax, which translocated to the mitochondrial membrane-inducing pores and stimulated a caspase cascade that eventually led to apoptosis (Fig. 8). The released Asp also caused downregulation of the anti-apoptotic genes.

The optimal Asp TLs displayed some extraordinary features. Despite containing a smaller drug dose, Asp TLs exposed to mild hyperthermia produced more substantial apoptotic effects

that were significantly higher than unloaded Asp. This has been proven by the remarkable increase in *Bak* and *Bax* levels, as well as the notable decline in *BCL-xL* and *BCL-2* levels upon exposure to the optimal Asp/TLs than free Asp (*P*-value <0.001).

Finally, it has been reported that the ideal temperature range for hyperthermia of cancer cells is from 38 °C (above physiological temperature) to 42 °C (above this temperature is harmful to healthy cells and not achievable in clinical settings).[74] The improved efficiency of Asp TLs combined with mild hyperthermia is attributed to the direct antitumor effect caused by mild heat through activating apoptotic pathways and intervening with DNA repair mechanisms. This leads to a synergistic interaction between the chemotherapeutic agent, Asp, and mild hyperthermia. Moreover, hyperthermia increases the tumor vascular permeability and, together with the EPR effect, aids in increasing the TLs intratumor accumulation. Finally, the vulnerability of tumor cells to mild heat has been reported to be caused by the more stressful conditions in cancer cells as compared to healthy ones, such as scarce nutrients, low oxygen levels, and tumor acidic microenvironments.[32,74]

4. Conclusion

In this study, thermoresponsive liposomes loaded with asplatin (Asp/TLs) were prepared and optimized using the Box–Behnken design in terms of size, PDI, zeta potential, and EE%. Then, the optimal formula was further characterized in terms of morphology, stability in physiological conditions, and temperature-dependent release manner. The optimized ASP/TLs exhibited nanoscale size, low PDI, outstanding surface charge, spherical morphology, and good entrapment efficiency. A gradual triggered release of Asp was observed from 38 °C until reaching the maximum release at 40 °C. Moreover, the optimal Asp/TLs displayed significantly higher cytotoxicity to MDA-MB-231 cells when exposed to 40 °C compared to the free Asp. The optimal Asp/TLs (40 °C) proved to be extremely effective at inducing both apoptosis and necrosis relative to free Asp (40 °C). This was further confirmed by the outstanding ability of Asp/TLs to induce the expression of the apoptotic genes; *Bak* and *Bax*, and the tumor suppressor gene *P53*, while reducing the expression of the anti-apoptotic genes *BCL-xL* and *BCL-2*.

Data availability

The data are contained within the article.

Conflicts of interest

The authors declare no conflict of interest.

Acknowledgements

This work was funded by the RSC Research Fund grant (ID: R22-3870733873) from the Royal Society of Chemistry to Dr Sherif Ashraf Fahmy.

References

1 WHO, *The Global Health Observatory*, 2023, accessed May 13, 2023, available from: **https://www.who.int/data/gho/data/themes/mortality-and-global-health-estimates/ghe-leading-causes-of-death**.
2 F. Bray, *et al.*, Global cancer statistics 2018: GLOBOCAN estimates of incidence and mortality worldwide for 36 cancers in 185 countries, *Ca-Cancer J. Clin.*, 2018, **68**(6), 394–424.
3 S. A. Fahmy, A. Ramzy, A. A. Mandour, S. Nasr, A. Abdelnaser and U. Bakowsky, Azzazy HME-S. PEGylated Chitosan Nanoparticles Encapsulating Ascorbic Acid and Oxaliplatin Exhibit Dramatic Apoptotic Effects against Breast Cancer Cells, *Pharmaceutics*, 2022, **14**(2), 407, DOI: **10.3390/pharmaceutics14020407**.
4 C. Zhang, *et al.*, Platinum-based drugs for cancer therapy and anti-tumor strategies, *Theranostics*, 2022, **12**(5), 2115.
5 A. A. Ali, C. M. McCrudden and H. O. McCarthy, Evaluation of the impact of nitric oxide on resistance to platinum-based chemotherapeutics, in *Nitric Oxide (Donor/Induced) in Chemosensitizing*, Elsevier, 2017, pp. 71–90.
6 I. Ritacco, *et al.*, Hydrolysis in acidic environment and degradation of satraplatin: a joint experimental and theoretical investigation, *Inorg. Chem.*, 2017, **56**(10), 6013–6026.
7 L. Kelland, The resurgence of platinum-based cancer chemotherapy, *Nat. Rev. Cancer*, 2007, **7**(8), 573–584.
8 D. P. Ballou, E. E. Trimmer and J. M. Essigmann, Cisplatin, *Essays Biochem.*, 1999, **34**, 191–211.
9 S. Dilruba and G. V. Kalayda, Platinum-based drugs: past, present and future, *Cancer Chemother. Pharmacol.*, 2016, **77**, 1103–1124.
10 J. Lokich and N. Anderson, Carboplatin versus cisplatin in solid tumors: an analysis of the literature, *Ann. Oncol.*, 1998, **9**(1), 13–21.
11 Q. Cheng, *et al.*, Asplatin enhances drug efficacy by altering the cellular response, *Metallomics*, 2016, **8**(7), 672–678.
12 S. A. Fahmy, *et al.*, Synthesis, Characterization and Host-Guest Complexation of Asplatin: Improved In Vitro Cytotoxicity and Biocompatibility as Compared to Cisplatin, *Pharmaceuticals*, 2022, **15**(2), 259.
13 L. Larasati, W. W. Lestari and M. Firdaus, Dual-Action Pt (IV) Prodrugs and Targeted Delivery in Metal-Organic Frameworks: Overcoming Cisplatin Resistance and Improving Anticancer Activity, *Bull. Chem. Soc. Jpn.*, 2022, **95**(11), 1561–1577.
14 R. G. Kenny, *et al.*, Platinum (IV) prodrugs – a step closer to Ehrlich's vision?, *Eur. J. Inorg. Chem.*, 2017, **2017**(12), 1596–1612.
15 H. Pandey, R. Rani and V. Agarwal, Liposome and their applications in cancer therapy, *Braz. Arch. Biol. Technol.*, 2016, **59**, 1–10.
16 F. Perche and V. P. Torchilin, Recent trends in multifunctional liposomal nanocarriers for enhanced tumor targeting, *J. Drug Delivery*, 2013, **2013**, 1–32.

17 C. Allen, *et al.*, Controlling the physical behavior and biological performance of liposome formulations through use of surface grafted poly (ethylene glycol), *Biosci. Rep.*, 2002, **22**, 225–250.
18 K. B. Sutradhar and M. Amin, Nanotechnology in cancer drug delivery and selective targeting, *Int. Scholarly Res. Not.*, 2014, **2014**, 1–12.
19 J. Lao, *et al.*, Liposomal doxorubicin in the treatment of breast cancer patients: a review, *J. Drug Delivery*, 2013, **2013**, 1–12.
20 Y. Malam, M. Loizidou and A. M. Seifalian, Liposomes and nanoparticles: nanosized vehicles for drug delivery in cancer, *Trends Pharmacol. Sci.*, 2009, **30**(11), 592–599.
21 R.-D. Hofheinz, *et al.*, Liposomal encapsulated anti-cancer drugs, *Anti-Cancer Drugs*, 2005, **16**(7), 691–707.
22 S. El-Shafie, *et al.*, Encapsulation of nedaplatin in novel pegylated liposomes increases its cytotoxicity and genotoxicity against a549 and u2os human cancer cells, *Pharmaceutics*, 2020, **12**(9), 863.
23 T. Ta and T. M. Porter, Thermosensitive liposomes for localized delivery and triggered release of chemotherapy, *J. Controlled Release*, 2013, **169**(1–2), 112–125.
24 M. Alawak, *et al.*, ADAM 8 as a novel target for doxorubicin delivery to TNBC cells using magnetic thermosensitive liposomes, *Eur. J. Pharm. Biopharm.*, 2021, **158**, 390–400.
25 J. Beik, *et al.*, Nanotechnology in hyperthermia cancer therapy: From fundamental principles to advanced applications, *J. Controlled Release*, 2016, **235**, 205–221.
26 A. Bettaieb, P. K. Wrzal and D. A. Averill-Bates, Hyperthermia: Cancer Treatment and beyond, in *Cancer Treatment-Conventional Innovative Approaches*, 2013, pp. 257–283.
27 P. Wust, *et al.*, Hyperthermia in combined treatment of cancer, *Lancet Oncol.*, 2002, **3**(8), 487–497.
28 T. M. Zagar, *et al.*, Hyperthermia for locally advanced breast cancer, *Int. J. Hyperthermia*, 2010, **26**(7), 618–624.
29 S. A. Fahmy, A. Ramzy, A. M. Sawy, M. Nabil, M. Z. Gad, M. El-Shazly, M. A. M. Aboul-Soud and H. M. E.-S. Azzazy, Ozonated Olive Oil: Enhanced Cutaneous Delivery via Niosomal Nanovesicles for Melanoma Treatment, *Antioxidants*, 2022, **11**, 1318, DOI: **10.3390/antiox11071318**.
30 O. M. Pijpers, *et al.*, Long-term efficacy of hyperthermic intravesical chemotherapy for BCG-unresponsive non-muscle invasive bladder cancer, in *Urologic Oncology: Seminars and Original Investigations*, Elsevier, 2022.
31 H. M. E.-S. Azzazy, *et al.*, Peganum harmala Alkaloids and Tannic Acid Encapsulated in PAMAM Dendrimers: Improved Anticancer Activities as Compared to Doxorubicin, *ACS Appl. Polym. Mater.*, 2022, **4**(10), 7228–7239.
32 S. A. Fahmy, *et al.*, Thermosensitive Liposomes Encapsulating Nedaplatin and Picoplatin Demonstrate Enhanced Cytotoxicity against Breast Cancer Cells, *ACS Omega*, 2022, **7**(46), 42115–42125.
33 A. A. Dayyih, *et al.*, Thermosensitive liposomes encapsulating hypericin: Characterization and photodynamic efficiency, *Int. J. Pharm.*, 2021, **609**, 121195.
34 A. Doyle, J. B. Griffiths and D. G. Newell, *Cell & tissue culture: laboratory procedures*, Wiley, 1998, vol. 3.
35 N. K. Sedky, *et al.*, The molecular basis of cytotoxicity of α-spinasterol from Ganoderma resinaceum: Induction of apoptosis and overexpression of p53 in breast and ovarian cancer cell lines, *J. Cell. Biochem.*, 2018, **119**(5), 3892–3902.
36 N. K. Sedky, *et al.*, Co-Delivery of Ylang Ylang Oil of Cananga odorata and Oxaliplatin Using Intelligent pH-Sensitive Lipid-Based Nanovesicles for the Effective Treatment of Triple-Negative Breast Cancer, *Int. J. Mol. Sci.*, 2023, **24**(9), 8392.
37 T. D. Schmittgen and K. J. Livak, Analyzing real-time PCR data by the comparative CT method, *Nat. Protoc.*, 2008, **3**(6), 1101–1108.
38 C. C. Cheung and W. T. Al-Jamal, Sterically stabilized liposomes production using staggered herringbone micromixer: effect of lipid composition and PEG-lipid content, *Int. J. Pharm.*, 2019, **566**, 687–696.
39 R. A. Youness, A. M. Al-Mahallawi, F. H. Mahmoud, H. Atta, M. Braoudaki and S. A. Fahmy, Oral Delivery of Psoralidin by Mucoadhesive Surface-Modified Bilosomes Showed Boosted Apoptotic and Necrotic Effects against Breast and Lung Cancer Cells, *Polymers*, 2023, **15**, 1464, DOI: **10.3390/polym15061464**.
40 A. A. Jovanović, *et al.*, Comparative effects of cholesterol and β-sitosterol on the liposome membrane characteristics, *Eur. J. Lipid Sci. Technol.*, 2018, **120**(9), 1800039.
41 Y. Wang, *et al.*, DPPC-cholesterol phase diagram using coarse-grained Molecular Dynamics simulations, *Biochim. Biophys. Acta, Biomembr.*, 2016, **1858**(11), 2846–2857.
42 L. Zhao, *et al.*, Preparation of liposomes using supercritical carbon dioxide technology: Effects of phospholipids and sterols, *Food Res. Int.*, 2015, **77**, 63–72.
43 Z. Hammoud, *et al.*, New findings on the incorporation of essential oil components into liposomes composed of lipoid S100 and cholesterol, *Int. J. Pharm.*, 2019, **561**, 161–170.
44 S. A. Fahmy, N. K. Sedky, A. Ramzy, M. M. M. Abdelhady, O. A. Alabrahim, S. N. Shamma and H. M. E. Azzazy, Green extraction of essential oils from Pistacia lentiscus resins: encapsulation into Niosomes showed improved preferential cytotoxic and apoptotic effects against breast and ovarian cancer cells, *J. Drug Delivery Sci. Technol.*, 2023, **87**, 104820.
45 C. Kim, *et al.*, Development of a single particle sizing system for monitoring abrasive particles in chemical mechanical polishing process, *J. Mech. Sci. Technol.*, 2023, **37**(3), 1317–1324.
46 R. Zhang, *et al.*, Nanobubble boundary layer thickness quantified by solvent relaxation NMR, *J. Colloid Interface Sci.*, 2022, **609**, 637–644.
47 F. Lenci, *et al.*, Spectroscopic and photoacoustic studies of hypericin embedded in liposomes as a photoreceptor model, *Photochem. Photobiol.*, 1995, **62**(1), 199–204.
48 S. Palchetti, The protein corona of circulating PEGylated liposomes, *Biochim. Biophys. Acta, Biomembr.*, 2016, **1858**(2), 189–196.

49 C. Gunawan, *et al.*, Nanoparticle–protein corona complexes govern the biological fates and functions of nanoparticles, *J. Mater. Chem. B*, 2014, **2**(15), 2060–2083.
50 S. S. Raesch, *et al.*, Proteomic and lipidomic analysis of nanoparticle corona upon contact with lung surfactant reveals differences in protein, but not lipid composition, *ACS Nano*, 2015, **9**(12), 11872–11885.
51 M. H. Gaber, *et al.*, Thermosensitive sterically stabilized liposomes: formulation and in vitro studies on mechanism of doxorubicin release by bovine serum and human plasma, *Pharm. Res.*, 1995, **12**, 1407–1416.
52 S. Ali, *et al.*, Wavelength dependent photo-cytotoxicity to ovarian carcinoma cells using temoporfin loaded tetraether liposomes as efficient drug delivery system, *Eur. J. Pharm. Biopharm.*, 2020, **150**, 50–65.
53 L. Li, *et al.*, Mild hyperthermia triggered doxorubicin release from optimized stealth thermosensitive liposomes improves intratumoral drug delivery and efficacy, *J. Controlled Release*, 2013, **168**(2), 142–150.
54 M. De Smet, *et al.*, Temperature-sensitive liposomes for doxorubicin delivery under MRI guidance, *J. Controlled Release*, 2010, **143**(1), 120–127.
55 T. M. Allen and P. R. Cullis, Drug delivery systems: entering the mainstream, *Science*, 2004, **303**(5665), 1818–1822.
56 S. A. Fahmy, H. M. E.-S. Azzazy and J. Schaefer, Liposome Photosensitizer Formulations for Effective Cancer Photodynamic Therapy, *Pharmaceutics*, 2021, **13**, 1345, DOI: **10.3390/pharmaceutics13091345**.
57 A. Gabizon, H. Shmeeda and Y. Barenholz, Pharmacokinetics of pegylated liposomal Doxorubicin: review of animal and human studies, *Clin. Pharmacokinet.*, 2003, **42**, 419–436.
58 M. B. Yatvin, *et al.*, Design of liposomes for enhanced local release of drugs by hyperthermia, *Science*, 1978, **202**(4374), 1290–1293.
59 D. Needham, *et al.*, A new temperature-sensitive liposome for use with mild hyperthermia: characterization and testing in a human tumor xenograft model, *Cancer Res.*, 2000, **60**(5), 1197–1201.
60 M. de Smet, *et al.*, Magnetic resonance imaging of high intensity focused ultrasound mediated drug delivery from temperature-sensitive liposomes: an in vivo proof-of-concept study, *J. Controlled Release*, 2011, **150**(1), 102–110.
61 Celsion, *Phase 3 Study of ThermoDox with Radiofrequency Ablation (RFA) in Treatment of Hepatocellular Carcinoma (HCC)*, 2014.
62 R. Lencioni, R. Ping Poon and C. Hua, *Study of Thermodox with Standardized Radiofrequency Ablation (RFA) for Treatment of Hepatocellular Carcinoma (HCC)(OPTIMA)*, ClinicalTrials. gov, 2014. Identifier: NCT02112656.
63 M. Alawak, *et al.*, Magnetic resonance activatable thermosensitive liposomes for controlled doxorubicin delivery, *Mater. Sci. Eng., C*, 2020, **115**, 111116.
64 W. J. Lokerse, *et al.*, Investigation of particle accumulation, chemosensitivity and thermosensitivity for effective solid tumor therapy using thermosensitive liposomes and hyperthermia, *Theranostics*, 2016, **6**(10), 1717.
65 N. M. Kholoussi, *et al.*, Evaluation of Bax and Bak gene mutations and expression in breast cancer, *BioMed Res. Int.*, 2014, **2014**, 1–9.
66 S. Krajewski, *et al.*, Reduced expression of pro-apoptotic gene BAX is associated with poor response rates to combination chemotherapy and shorter survival in women with metastatic breast adenocarcinoma, *Cancer Res.*, 1995, **55**(19), 4471–4478.
67 M. Schuyer, *et al.*, Reduced expression of BAX is associated with poor prognosis in patients with epithelial ovarian cancer: a multifactorial analysis of TP53, p21, BAX and BCL-2, *Br. J. Cancer*, 2001, **85**(9), 1359–1367.
68 A. Levine, W. Hu and Z. Feng, The P53 pathway: what questions remain to be explored?, *Cell Death Differ.*, 2006, **13**(6), 1027–1036.
69 T. Riley, *et al.*, Transcriptional control of human p53-regulated genes, *Nat. Rev. Mol. Cell Biol.*, 2008, **9**(5), 402–412.
70 M. Kvansakul and M. G. Hinds, The Bcl-2 family: structures, interactions and targets for drug discovery, *Apoptosis*, 2015, **20**, 136–150.
71 Z. N. Oltval, C. L. Milliman and S. J. Korsmeyer, Bcl-2 heterodimerizes in vivo with a conserved homolog, Bax, that accelerates programed cell death, *Cell*, 1993, **74**(4), 609–619.
72 M. Sattler, *et al.*, Structure of Bcl-xL-Bak peptide complex: recognition between regulators of apoptosis, *Science*, 1997, **275**(5302), 983–986.
73 R. M. Mohammad, *et al.*, Preclinical studies of a nonpeptidic small-molecule inhibitor of Bcl-2 and Bcl-XL [(−)-gossypol] against diffuse large cell lymphoma, *Mol. Cancer Ther.*, 2005, **4**(1), 13–21.
74 P. Vaupel, H. Piazena, M. Notter, A. R. Thomsen, A.-L. Grosu, F. Scholkmann, A. G. Pockley and G. Multhoff, From Localized Mild Hyperthermia to Improved Tumor Oxygenation: Physiological Mechanisms Critically Involved in Oncologic Thermo-Radio-Immunotherapy, *Cancers*, 2023, **15**, 1394, DOI: **10.3390/cancers15051394**.